The 2010 IEEE/RSJ International Conference on
Intelligent Robots and Systems
October 18-22, 2010, Taipei, Taiwan

Collecting an Object by Casting Manipulation

Hitoshi Arisumi, and Kazuhito Yokoi, *Member, IEEE*

***Abstract*— We have been developing a casting manipulator that includes a flexible light wire in the link mechanism to enlarge the workspace of the manipulator. In this paper we focus on the motion of collecting an object via casting manipulation. We propose a method of moving the object in the air by coordinating the motions of swinging the arm and winding the wire. Then, we develop a mechanical device that changes the apparent elasticity of the wire to transmit force to the object effectively. We also develop the motion generator that provides the optimal collect motion. We confirm the effectiveness of the proposed method through simulations. Finally, we conduct experiments using casting manipulator hardware and realize the quick motion of collecting the object.**

***Index Terms*— manipulation, elastic wire, impulsive force, midair trajectory control**

I. Introduction

A. Background

A large workspace is one of the basic features required in robotic manipulation, especially for filed works. Figure 1 qualitatively shows the workspace of typical robot manipulators for various landforms. The workspace of fixed manipulators such as industrial manipulators is restricted by the length of their arms, which are several meters long at most. Mobile manipulators, such as wheeled or legged robot manipulators are possible means for enlarging the workspace via their mobility; however, it is still difficult for them to move through wasteland containing features such as deep depressions, steep slopes, or swamps, as shown in Fig. 1. To overcome this difficulty, we have previously proposed the method of enlarging workspace of manipulators by replacing several of the rigid links with a light, flexible wire. The proposed system, called "a casting manipulator," [1] consists of a rigid arm, a flexible wire with variable length, and a gripper as shown in Fig. 1(d). Figure 2 shows the phases of the casting manipulation motion to catch a target object. First, the arm swings repeatedly to build up kinetic energy [1]. Next, the gripper is launched to the target by changing the length of the wire [2]. While the gripper flies, its trajectory is controlled by the tension in the wire [3], [4]. Finally, the gripper approaches the target in a suitable state and catches the target object [5]. In this way, the casting manipulator obtains a large workspace by making effective use of its dynamics. This manipulator uses substantially less energy to move the gripper with high speed as compared to other robot designs; additionally it has a light and compact body for transportation thanks to its simple mechanism and low power. Therefore, it can be expected to be applied to fieldwork such as collecting samples for examination of volcanic activity in locations people cannot easily approach or for interplanetary exploration. It may also be used for other applications such as land survey, maintenance of large bridges, or rescue/recovery works for disaster area.

For many of these applications, it is also necessary to pull the gripper back to the base of the robot after reaching the target. In this paper, we consider suitable strategies for collecting the gripper.

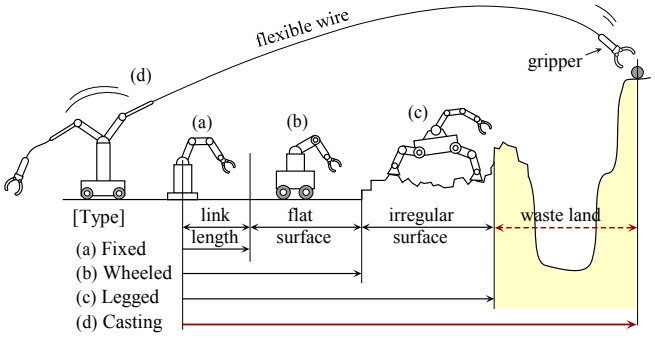

Fig. 1. Workspace of robots

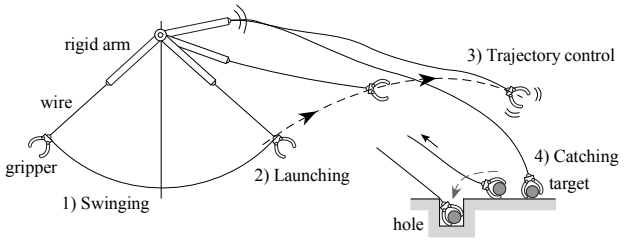

Fig. 2. Phases of the casting manipulation.

B. Related Works

Many off-road vehicles are equipped with winches, the use of which can be considered as collecting an object by winding a wire. They are well suited to moving heavy objects slowly, but drag the objects along the ground. Hence, if there is a hole or a hook on the ground, the object may fall into the hole and get stuck as shown in Fig. 2, or the wire may become entwined on the hook. In this case, it is difficult to move the object only by pulling the wire. When the wire is pulled more strongly, the object or the wire may get damaged. To avoid this situation, it

Manuscript received February 22, 2010. This work was supported in part by the Japan Society for the Promotion of Science under Grant-in-Aid for Scientific Research (B) 21360122.

H. Arisumi (Corresponding Author), and K. Yokoi are with the Intelligent Systems Research Institute of the National Institute of Advanced Industrial Science and Technology (AIST), Tsukuba Central 2, 1-1-1 Umezono, Tsukuba, Ibaraki 305-8568, Japan. Contact TEL: +81-29-861-7282 FAX: +81-29-861-5444 e-mail: h-arisumi@aist.go.jp

is desirable to find a method that is independent of the shape of the ground such as moving the object in the air.

Several kinds of a wire-driven robot such as parallel-wired robot or travelling crane robot have been developed [6], [7]. They can move the object through the air, but the carriage rail or reel system must be placed in the environment between the robot and the target object. Therefore these systems are not suited for the fieldwork application mentioned above. Moreover because they rely on antagonistic actuation, they cannot expand their work space out of space which is enclosed by the distributed devices such as reel systems.

C. Research Target

In this paper, we address the mid-air control of the collected object to keep it from the ground, and discuss its motion generation and control method. We also propose a mechanical system for implementing the motion and develop the casting manipulator hardware including this system. We finally realize the motion of collecting the object through both simulations and experiments.

II. Strategy for Collecting An Object

Here, we discuss three points: how to pull the wire to keep the object away from the ground during its flight, how to generate enough energy for the object to reach the base of the robot, and how to catch the object when it flies back to the base.

A. How to Pull the Wire?

Considering the driving system of the casting manipulator, there are two ways of pulling the wire: (a) swinging the arm and (b) winding the wire as shown in Fig. 3. The merits and drawbacks of each motion are follows.

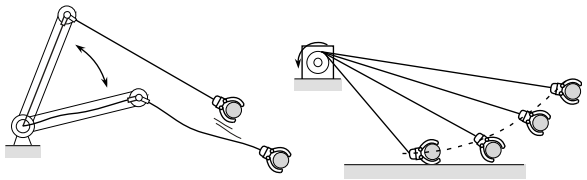

(a) Swing of the arm (b) Wind of the wire

Fig. 3. Ways of pulling the wire.

(a) Swinging the arm: A large force can be applied to the wire by using the inertia of the arm. It can pull the wire from various directions by changing the angle of the arm. Then, by pulling the wire from the higher position, it can increase the upper speed of the object which is available for a flight of the object. However, the length of the wire between the arm and the gripper cannot be shortened only by this motion.

(b) Winding the wire: A high-power actuator is necessary to generate a large force instantly because it is hard to use the motor's inertia effectively. When pulling the wire at the constant actuator velocity, the object falls to the ground as shown in Fig. 3(b) because the upward force is not applied to the gripper. To avoid this falling, the reel system must keep accelerating the winding motion, but the extent to which this is possible is limited by the maximum angular velocity of the winding actuator.

Considering these merits and drawbacks, we take the approach of using the two motions to complement each other, first swinging the arm to pull the wire and then shortening it by winding it in. Here, we protect the reel system from large tensions by applying the swinging and winding motions sequentially rather than simultaneously. During swinging, the wire is held in place by a brake.

The next discussion is how to transmit the energy of swing motion to the object most effectively. For example, let us take the severe case of lifting a heavy object by swing motion. Assuming that the torque of the actuator is weaker than the weight of the object, the actuator may become saturated when lifting an object. When lifting the object statically in the saturated area, the arm gets unstable and falls down as shown in Fig. 4(a). To mitigate this saturation, we use a preliminary motion of the arm as shown in Fig. 4(b). The swing motion imparts momentum to the arm while the wire is slack. This momentum allows the arm to apply an impulsive force to the object when the string goes taut; if this impulse is large enough, the arm can pass through the saturated area and into the unsaturated area B. This method is good for lifting an object dynamically without using the high-power actuator indeed, but the energy may be dissipated due to the damping effect of the inextensible wire. To address this matter, we consider an additional elastic effect in the wire. In case of the wire with spring shown in Fig. 4(c), the extension of the wire allows the arm to move through the saturated area under a smaller load. When the arm reaches the upper unsaturated area B, the heavy object can be lifted by the restoring force of the spring as shown in Fig. 4(d).

In this paper, we use both inertial effects and elastic effects for pulling the wire.

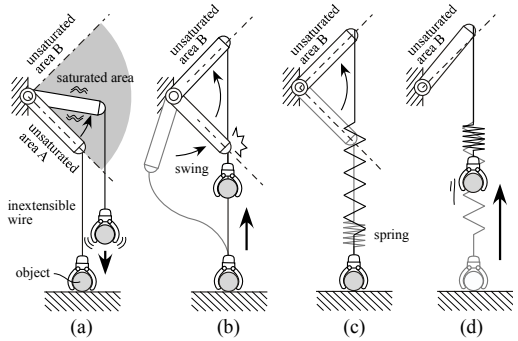

Fig. 4. Effective way of lifting an object to higher position.

B. How to Provide Elastic Effect for the Wire?

The next question we should ask is how to provide the elastic effect in the wire. We consider a direct way as shown in Fig. 5(a), and indirect ways as shown in Figs. 5(b)-(d). The directly elastic wire shown in Fig. 5(a) has a negative effect on the other phases of the casting manipulation such as swinging or throwing as illustrated in Fig. 2. In general, the stretching and compression of the wire can yield a complicated swing

motion and disturb the throwing control. Furthermore, it is difficult to measure the expansion of the wire. Consequently, this approach (a) is not a good choice. For the same reason, we do not use a flexible arm as shown in Fig. 5(b). Instead, we use an inextensible wire and a separated spring as in methods (c) and (d). Each of these basic implementations has its own problems, however. In the method (c), bending of the wire causes friction at the pulleys, which disturbs the motion of the wire at the high speed. In method (d), the reel system generates large inertial and frictional forces due to its weight, which also reduce the elastic effect at the gripper.

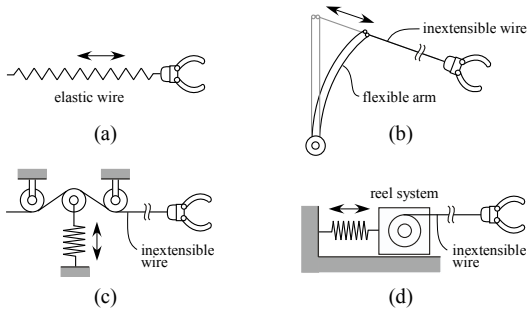

Fig. 5. How to provide the elastic effect for the wire?

To solve these problems, we propose the spring-slider-brake (SSB) system shown in Fig. 6. This system consists of an inextensible wire, a slider that moves along the arm, the brake on the slider for holding the wire, a spring that connects the slider and the base of the arm, a hook for arresting the slider, and an unlocking device. This system has three chief merits:

- The apparent elasticity of the wire can be controlled
- It has a long stroke for giving the elastic effect to the gripper
- The inertial load of the slider is smaller than for alternative systems

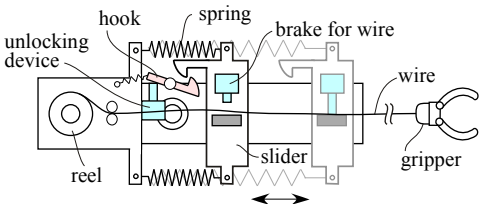

Fig. 6. Structure of the spring-slider- brake (SSB) system.

C. Target Motion

We here describe how to collect an object by using the SSB system. The target motion is shown in Figs. 7(a)-(f).

State (a) shows the preliminary motion of the arm, swinging the arm while the wire is loose.

State (b) shows the start of pulling the wire. At that time, the hook is unlocked by actuating the unlocking device to free the slider. At the same time, the wire is held by the brake equipped on the slider.

State (c) shows the spring of the system at full expansion. From the viewpoint of the gripper, the wire stretches as if the wire is elastic.

State (d) shows the slider having returned to its initial position quickly because of the restoring force of the spring. The gripper has accelerated quickly during this motion.

State (e) shows the free flight of the gripper. The slider is locked again, and the wire is released by turning off the brake system. The wire is wound in by the reel system.

State (f) shows the end of this motion cycle, with the arm swinging back to its initial position.

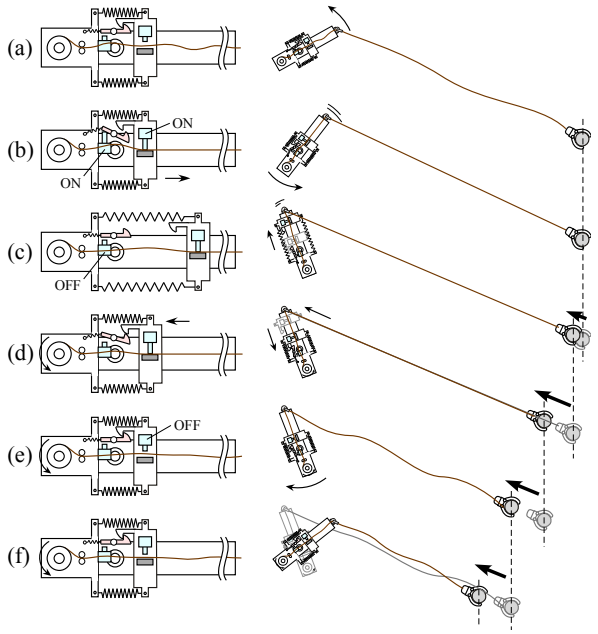

Fig. 7. Target motion.

D. How to Generate Enough Energy to Fly to the Base?

In case of collecting a heavier object or an object from further away, a single swing of the arm may not generate enough energy for the object to reach the robot's base. We now apply the energy-pumping principle to the collection motion. We propose a repetitive cooperative motion of the arm and the reel system as shown in Fig. 8. We can expect that this motion is realized by repeating the target motion in Fig. 7. The object would approach the robot's base as if the object bounds through the air.

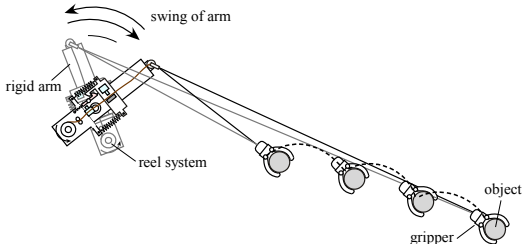

Fig. 8. Repetitive cooperative motion of the arm and the reel system.

E. How to Catch the Object?

The object may approach the robot's base at the high speed in the collection motion. If the robot does not catch it at the end of the motion, the object may collide with the main body of the robot such as the rigid arm. In this case, the system and the object are likely to be damaged. To avoid this, the robot

should ensure that the object finishes in a statically or dynamically stable state. As an example of the dynamically stable sate, we consider the swing motion such as phase 1) in Fig. 2. If the robot can connect the collection motion to the swing motion, it can make good use of kinetic energy of the object for the next throw motion. Then, the robot could successively throwing the collected object to the other place and put it on there. In the next section, we address how to generate the stable cyclic motion by using the flight motion of the object.

III. Motion Generation and Control

We discuss here how to generate and control the collect motion in the vertical plane by making use of the SSB system. Focusing on the impulsive motion, we regard the gripper and the object as a mass point for simpler discussion in this paper. We call them just 'object' from here on.

A. Model of the System and Dynamic Equations

Figure 9 shows a model of the whole system. Instead of omitting description of slider and brake, we describe them as the shaded part as shown in Fig.9. The shaded part represents the three states of the mechanical part connected with the wire: (a) the spring of the SSB system, (b) taut wire, and (c) slack wire. They are switched by activating the brake and the hook in Fig. 6. J_1, J_2, and G in Fig. 9 are the positions of joints 1, 2, and the center of gravity of the object, respectively. J_1 has absolute coordinates $(0, L_0)$. L_1 is the length of link 1. L_{g1} is the distance between J_1 and the center of gravity of link 1. m_1 and m_3 are the masses of the link 1 and the object, respectively. I_1 is the moment of inertia of link 1 around J_1. d_w is the distance between the reel and J_2, and r_{w0} is the distance between J_2 and G just before applying the brake to the wire.

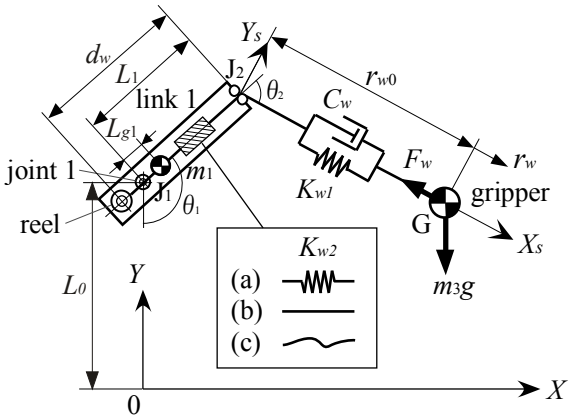

Fig. 9. Model of casting manipulator

The orthogonal coordinate system, $O - X_sY_s$, is set on the wire so that the origin of $O - X_sY_s$ is located on J_2, and the direction of X_s axis agrees with that of the wire. r_w is the displacement of point G in the direction of X_s axis. θ_1 is the angle between the vertical line and X_s axis. We consider the negative direction of Y axis to be the direction of the gravitational force.

We are concerned here with the dynamics of the system in the case of spring, state (a) in Fig. 9. In this case, the wire is held by the brake, and the hook is unlocked as shown in Fig. 6. Since the flexible wire does not transmit moment, only force in the direction of X_s axis can be applied to the object. We thus divide the object motion along the directions of the X_s and the Y_s axes. The dynamic equations of the object are obtained as follows:

$$m_3 (\ddot{r}_w - (r_{w0}+r_w) \dot{\theta}_{12}{}^2 - \xi_1{}^2 L_1 C_2 - \xi_2 L_1 S_2) = m_3 g C_{12} - F_w \quad (1)$$

$$m_3 (2\dot{\theta}_{12}\dot{r}_w + (r_{w0}+r_w) \ddot{\theta}_{12} - \xi_1{}^2 L_1 S_2 + \xi_2 L_1 C_2) = -m_3 g S_{12}, \quad (2)$$

where $\theta_{12} = \theta_1 + \theta_2$, $C_i = \cos\theta_i$, $S_i = \sin\theta_i$, $\xi_1 = \dot{\theta}_1 + \dot{\theta}_{12}$, $\xi_2 = \ddot{\theta}_1 + \ddot{\theta}_{12}$, and F_w is tension of the wire. Letting K_{wi} $(i = 1, 2)$ be the spring stiffness, C_w be the viscous damping coefficient of the wire, and r_i $(i = 1, 2)$ is the extension of the spring i as shown in Fig. 9, we obtain

$$F_w = K_{w1}\, r_1 + C_w \dot{r}_1 = K_{w2}\, r_2 \quad (3)$$

$$r_w = r_1 + r_2. \quad (4)$$

Eliminating r_1 and r_2 from (3) and (4), the dynamic equation of the wire is expressed by the following:

$$(K_{w1} + K_{w2})\, F_w + C_w \dot{F}_w = K_{w1}\, K_{w2}\, r_w + K_{w2}\, C_w \dot{r}_w , \quad (5)$$

B. Control of the Arm

We use an asymmetric cycloidal curve, chosen as one of the cam curves in [8], [9], for the reference trajectory of joint 1. The asymmetric cycloidal curve is described as follows:

$$S(T) = T - \frac{T_a}{\pi} \sin \frac{\pi T}{T_a} \quad (0 < T < T_a)$$

$$S(T) = T + \frac{1-T_a}{\pi} \sin \frac{T-T_a}{1-T_a} \pi \quad (T_a < T < 1) \quad (6)$$

where T and T_a are the dimensionless time and the dimensionless parameter of time at the maximum velocity of this cam curve, respectively. The $S(T)$ of this cam curve changes from 0 to 1 smoothly. In general, this cam curve is used for the high speed motions of mechanical systems because it causes minimal vibrations. Using $S(T)$, the reference trajectory of angle of joint 1, θ_{1ref}, is given by

$$\theta_{1ref} = \theta_{amp}\, S(t/t_f), \quad (7)$$

where t_f and θ_{amp} represent the duration and the maximum displacement, respectively. The reference trajectory of angular velocity and acceleration, $\dot{\theta}_{1ref}$ and $\ddot{\theta}_{1ref}$, are derived by differentiating (7). These parameters of the reference trajectory are used for the computed torque method to control joint 1. The control torque τ_1 is given by

$$\tau_1 = I_1 \{ \ddot{\theta}_{1ref} + k_v (\dot{\theta}_{1ref} - \dot{\theta}_1) + k_p (\theta_{1ref} - \theta_1) \} + \tau_{gv} - \tau_{ext} \quad (8)$$

where τ_{gv} and τ_{ext} are the gravitational torque and the external torque for joint 1, the latter of which is caused by the tension F_w in the wire. k_v and k_p are the proportional gain and the derivative gain, respectively.

C. Desired Trajectory of the Flying Object

Figure 10 shows the motion of the arm and the object when collecting the object. The object is pulled by repetitive swing of the arm as described in Section II-D. Point P_i represents the object's position at a time $t_a(i)$, where i is the number of the swing motion. Figures 10(a)-(c) correspond to Figs. 7(a)-(c), respectively. The swing from (a) to (b) represents the preliminary motion for applying impulsive force to the object. In Fig. 10, θ_{1a}, θ_{1b}, θ_{1c}, and θ_{1d} represent the angles of the arm (a)-(d) at the time $t_a(i)$, $t_b(i)$, $t_c(i)$, and $t_d(i)$, respectively. At time $t_b(i)$, the arm starts to pull the object. After finishing the pull at time $t_c(i)$, the arm moves to the initial position (d) of the next swing. The i^{th} swing finishes at time $t_d(i)$, which is also the start time $t_a(i+1)$ of swing $i+1$. The object flies from initial position P_0, changing its direction at each P_i. Between each change of direction, the object traces a ballistic trajectory, represented as a thick dotted line in Fig. 10. The reference trajectory of joint 1 for the swing from (a) to (c) is obtained by substituting $t_f = t_c - t_a$ and $\theta_{amp} = \theta_{1c} - \theta_{1a}$ into (7).

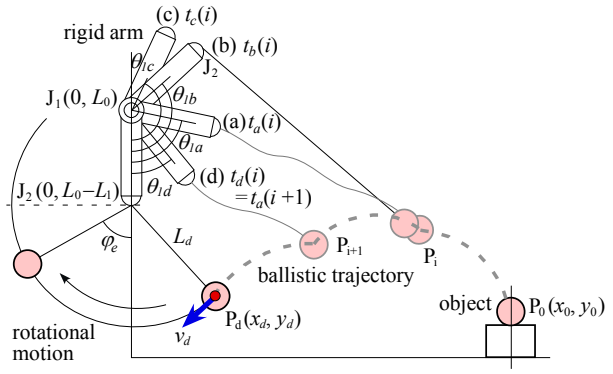

Fig. 10. Motion of the arm and the object when collecting the object.

When the object reaches the robot's base, the robot should control the object's trajectory to catch it. To achieve this control, we consider how to convert a ballistic motion of the object into a cyclic motion. This is our dynamically goal stable state discussed in Section II-E. For simplicity, the arm is placed at $\theta_1 = 0$ when the cyclic motion starts. The reference trajectory of joint 1 for the swing from (c) to (d) is obtained by substituting $t_f = t_d - t_c$ and $\theta_{amp} = \theta_{1d} - \theta_{1c}$ into (7). In Fig. 10, P_d is the connecting point between ballistic trajectory and cyclic motion. For a smooth connection, the direction of the object's speed at P_d should be the same as the tangent of the arc of the cyclic motion. Therefore, the relation between the position of P_d and the direction of the object's speed at P_d is expressed by the following equation:

$$\alpha_d = \frac{\dot{y}_d}{\dot{x}_d} = \frac{x_d}{(L_0 - L_1 - y_d)} \tag{9}$$

where α is the gradient of the object's speed v_d at P_d, (x_d, y_d) are the coordinates of P_d, and $(\dot{x}_d, \dot{y}_d)$ are the xy components of v_d.

D. Constraints

The constraints implemented in the motion optimization must be satisfied with the following inequalities:

$$|\tau_1| < \tau_{max} \tag{10}$$
$$|\dot{\theta}_1| < \omega_{max} \tag{11}$$
$$|F_w| < F_{max} \tag{12}$$
$$|\varphi_e| < \varphi_{max} \quad \text{or} \quad |\varphi_e| > \varphi_{max} \tag{13}$$

where τ_{max} and ω_{max} are the maximum torque and angular velocity of the actuator, F_{max} is the maximum allowable tension of the wire, and φ_e is the maximum swing angle. The former constraint in (13) is for the pendulum swing, while the latter is for the one-way rotational motion. Additional constraint is that there be no geometrical interference between the robot and the object. We further assume that the frictional coefficient of the floor is large enough to prevent the object from sliding.

E. Optimization

There are many combinations of ballistic and cyclic trajectories that are smoothly connected. To define both trajectories, we set the connecting point P_d by hand. Once given x_d and y_d, the gradient α_d is calculated by (9). We regard (x_d, y_d, α_d) as the target state S_d of the object at P_d. We discuss here how to make the object reach this target state.

When the object is pulled by multiple swing of the arm, it flies between its initial and final states. In other words, the control parameters on the arm's swing define the object's trajectory and its final state. The control parameters are denoted by $U_C(t_c - t_a, t_d - t_c, \theta_{1a}, \theta_{1b}, \theta_{1c})$. In case of an n-times swing, they are a set of ${}^1U_C, \cdots, {}^nU_C$. When given this set, the object's ballistic trajectory is fully specified. The ballistic trajectory is composed of two motions; the motion when the object is pulled and the free-fall motion. The former is calculated numerically by using (1), (2) and (5). Then, the final state of the object $S_f(x_f, y_f, \alpha_f)$ when $x_f = x_d$ can be derived. We here define the distance between the target state and the final state, $D(S_d, S_f)$, as follows:

$$D(S_d,S_f)=c_1(x_d-x_f)^2+c_2(y_d-y_f)^2+c_3(\alpha_d-\alpha_f)^2, \tag{14}$$

where c_i (i = 1,2,3) are weighting factors. By minimizing this function (14) under the constraints (10)-(13), we can obtain the optimal control parameters. The number of arm swings n may depend on the distance to the target and the possible distance achievable with a single swing. We here deal with a short distance of a target, and search for the feasible solution with increasing the number n until the objective function converges sufficiently. The quasi-Newton method is used for optimization, and the self-scaling variable metric (SSVM) algorithm [10] is used for improving its convergence.

IV. SIMULATION

A. Lifting Motion

We verify the effect of the arm's inertia and the wire's elasticity which is described in Section II-A.

We consider two wire models, Figs. 9(a) and (b), for lift of the heavy object. The arm swings from state (a) in Figs. 10 to state (c), and pulls the wire at state (b). The initial position of the object is set as $P_0(x_0, y_0) = (L_1 \sin\theta_{1b}, 0)$. We examine the highest lift position of the object achieved with variations in the control parameters $U_L(t_c, \theta_{1a}, \theta_{1b}, \theta_{1c})$ within their limits. The specifications for the simulation are the followings: $m_1 =$ 3.86kg, $m_3 = 1.5$kg, $L_0 = 1.69$m, $L_1 = 0.48$m, $L_{g1} = 0.021$m, $I_1 =$ 0.22035kgm^2, K_{w1} = 4940.0N/m, C_w = 52.0Ns/m, τ_{max} = 2.0Nm, ω_{max} = 1800deg/s, F_{max} = 592.9N, $T_a = 0.55$. We set the spring stiffness for wire models (a) and (b) in Fig. 9 as K_{w2} = 78.0N/m and $K_{w2} = 13300.0$N/m, respectively.

Figure 11 shows (a) angle of joint 1, (b) torque of joint 1, (c) height of the object, and (d) tension in the wire, respectively. The thin dotted lines and solid lines in Fig. 11 represent the case that only the effect of the arm's inertia is used for lifting with the wire model (b) in Fig. 9. The thick dotted lines represent the case that both effects are used for lifting with the wire model (a). Each line represents the lift motion controlled by each U_L as described in the caption of Fig. 11. Two horizontal dashed lines in Fig. 11 (a) represent the boundary of the saturation area. The upper and lower boundary angles are 108.1deg and 71.9deg, respectively. The two boundary torques in Fig. 11(b) are ±7.5 Nm. In Fig. 11 (a), the thin dotted line cannot cross over the saturation area because of ineq. (10). Then the arm stops at the lower boundary angle. Instead of (10), we give the following conditions for lift only by the inertial effect: $\tau_1 = \tau_{max}$ (if $\tau_1 > \tau_{max}$), and $\tau_1 = -\tau_{max}$ (if $\tau_1 < -\tau_{max}$), where τ_1 is command torque. The solid line represents the lift motion under these conditions.

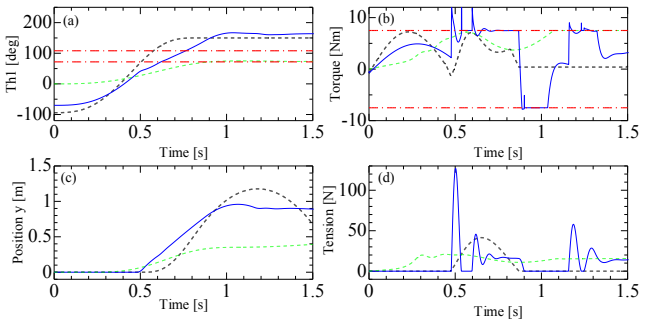

Fig. 11. Lift motion of the object. Thin dotted line (green): U_L(1.10, 0.0, 0.0, 80.0), Solid line (blue): U_L(0.97, -70.0 32.0 164.0), Thick dotted line(black): U_L(0.82, -94.0 54.0 158.0).

As shown in Fig. 11(a), the arm crosses over the saturation area, but the actual torque has several peaks over the upper bound as shown in Fig. 11(b). At these peaks, the large tension is applied as shown in Fig. 11(c). In case of using both the arm's inertia and elasticity of the SSB system for dynamic lift, the arm cross over the saturation area without saturation of the actual torque as the thick dotted line in Figs. 11(a) and (b). Then, the robot lifts the object to a height of 1.288m as shown in Fig. 11(c). This is the highest position for this system and the control method under the specified conditions. When the tension is zero, it means the object is on the floor before pulling or the object is free-falling. In Fig. 11(d), the tension changes smoothly and decreases.

We found that the inertial effects are not enough to lift the heavy object, and the proposed system improves maximum lift height by using the elastic effect together with the inertia.

B. Collecting an Object

To prove the validity of our new mechanism and its control method, we carried out tests with the dynamic simulator. We discuss here the use of inertial and elastic effects for pulling an object as described previously, using the same parameters as in the example in Fig. 10.

We consider two cases with initial positions of the object set as $(x_0, y_0) = (2.0\text{m}, 0.32\text{m})$ and (4.0m, 0.32m) for tests (A) and (B), respectively. The target position and gradient are set as $S_d(x_d, y_d, \alpha) = (0.5\text{m}, 0.4\text{m}, 0.6173)$ in both cases. These conditions are described in Section IV-A.

We obtain the optimal control parameters that minimize (14) as described in Section III-E. In the case of the test (A) is 2.0m, $U_C(t_c - t_a, t_d - t_c, \theta_{1a}, \theta_{1b}, \theta_{1c}) =$ (0.560s, 0.337s, 56.0deg, 107.0deg, 138.0deg), $D(S_d, S_f) = 0.028963$ when $c_1 = c_2 = 200$, $c_3 = 100$, and $\varphi_{max} = 90$deg for the former inequality of (13). In the case of the test (B), the feasible solution is given when $n =$ 2; ${}^1U_C$ = (0.193, 0.040, 120.8, 132.5, 170.7), ${}^2U_C$ = (0.222, 0.219, 78.7, 96.7, 185.3), $D(S_d, S_f) = 0.474224$ when $c_1 = c_2 =$ 200, $c_3 = 100$, and $\varphi_{max} = 270$deg for the later inequality of (13). The computational times on the PC (1.80GHz CPU Intel Core2 Duo) are 1.13s and 1.46s for the test (A) and (B), respectively.

Figure 12 shows the trajectories of the object. The solid line in the figure is the result for the test (A), and the thick dotted line is that for (B). The triangles represent the initial positions of the object, while the circle and the square denote the target position and the position of joint 2 in the final state of the arm, respectively. The dashed diagonal line represents the desired gradient at the target point.

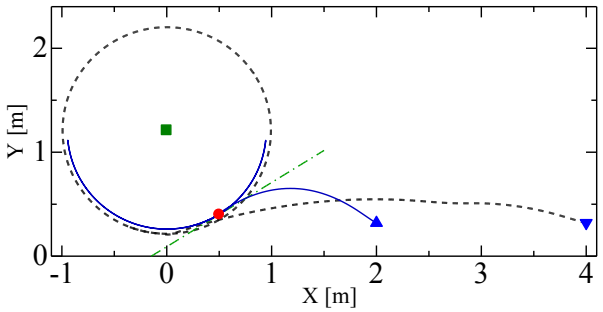

Fig. 12. Optimal trajectory of the object.

In Fig. 12, the shape of the ballistic trajectory is not always parabolic because of acceleration of the object due to the

string tension. In the test (A), the object reaches the target point very closely, and the ballistic and pendulum trajectories are smoothly connected. In the test (B), the trajectory does not pass through the target point because of insufficient convergence of the optimization. However, the rotational motion is generated by the constraint (13). We also confirmed that both cyclic motions are stable. Note that the convergence may be improved by changing the weighting factors of the objective function or increasing number of the arm swings. We will discuss on this matter as a future work.

Figure 13 shows the *x*-*y* coordinates of the object, the gradient of its velocity, and the spring/wire extension with respect to time. The left side of the figures shows results for the test (A) and the other side shows those for the test (B). The red circles denote the target position and gradient. The vertical dashed line represent the start time of pulling the object. The times of these vertical dashed lines in the left and right figures are 0.374s and 0.073s, respectively. Before these times, the preliminary motion of the arm is generated as in Figs. 7(a)-(b). After these times, extension of the spring and wire increases as shown in Fig. 13(c) and (f). The period while extension is positive corresponds to (b)-(d) in Fig. 7. After the extension becomes almost zero, the arm moves from Fig. 7(e) to (f). Since the object is pulled two times in test (B), the wire extends two times as shown in Fig. 13(f).

From the *x*-*y* curves in Fig. 13(a), (d), the time when the object starts moving is later than the dashed line. This means the spring stretches before the object's motion. The gradient α is increasing while the object on the ballistic trajectory approaches the target point. On the other hand, it is decreasing while the object on the pendulum trajectory leaves the target point. Therefore, the gradient α does not change smoothly around the target point as shown in Fig. 13(b) and (e).

The wire stretches and shrinks a small amount after passing through the target point as shown in Fig. 13(c) and (f). The object may receive an impact at that time, but it does not have significant effect on the motion of the object as shown by the trajectory in Fig. 12.

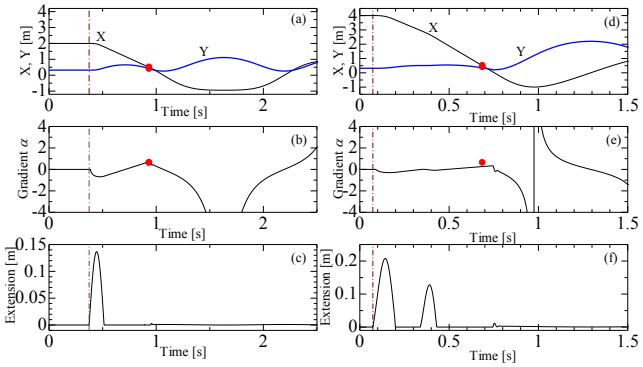

Fig. 13. The x-y coordinates of the object, the gradient of its velocity, and extension of the spring/wire.

Due to space limitation, only screenshots of the simulation test (A) are presented in Fig. 14. Note that the wire is loose from (a) to (b) and from (c) to (d), contrary to its illustration. In the figure, the arm moves from the initial state (a) to the state (b) to generate its kinetic momentum. Then the arm reaches the end of the counter clockwise swing (c). In (d), the arm moves downward with rewinding the wire. The object is free in the air at that time. Both arm and object reaches their own target position at the same time (e). Finally the arm is fixed, and the pendulum swing is generated around the tip of the arm (f). Since the maximum swing angle of the pendulum is less than 90deg, the swing is stable.

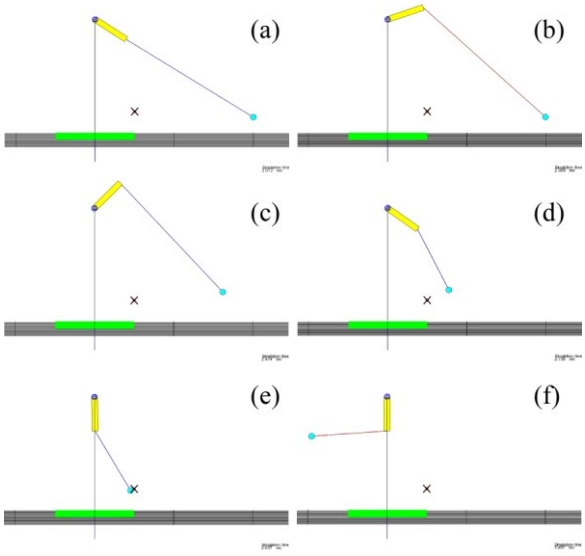

Fig. 14. Simulation results of the collect motion.

V. EXPERIMENT

A. Hardware

We developed the casting manipulator system shown in Fig. 15. The rigid arm is driven by a DD motor attached at its base. The reel is also driven by a DD motor attached at the rigid arm. The angle of the DD motor is measured by an optical encoder. We use a softball attached at the tip of the wire as the object collected. The SSB system is equipped on the rigid arm as shown in Fig. 15. In Fig. 16, two springs connect the slider and the fixed bar on the rigid arm, and the hook is equipped at the center of the two rails.

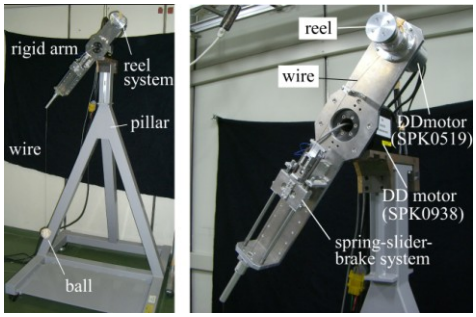

Fig. 15. Overview of the casting manipulator.

The specification of the device is given in Table I. This system runs on a 1GHz CPU-based PC (Intel Pentium(R) III) under real time OS, ART-Linux 2.4.34. The sampling time is set at 0.001s.

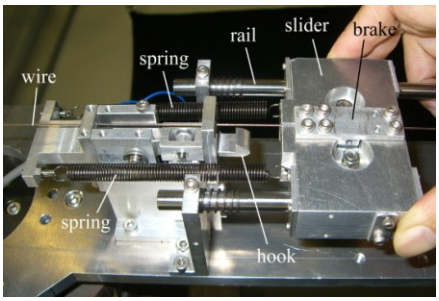

Fig. 16. Hardware of the spring-slider- brake (SSB) system.

TABLE I
SPECIFICATION OF THE DEVICES

DD motor SPK0938	Rated Torque	Max Torque	Max Speed	Encoder
	2.1Nm	7.5Nm	300rpm	18,000p/rev
DD motor SPK0519	Rated Torque	Max Torque	Max Speed	Encoder
	0.22Nm	0.54Nm	2400rpm	5,000p/rev
Solenoid 4EFP (Shindengen Corp.)		Power 50W	Max Force 114N	
Wire: fishing line for salt water (Sunline Corp.)		Hyper polymer polyethylene		Max: 60.5kg

B. *Collecting an Object*

We conducted experiments on the test (A) under the same conditions as Section IV-B. Figure 17 shows the sequential motion of collecting a ball by the casting manipulator. Comparing to Fig. 14, experimental results almost agree with simulation results except for (e) in Fig. 17. In (e), the arm does not reach the target position precisely when the ball reaches the target point. To reduce the delay of the arm, we need to improve the response of the controller for its actuation. If this delay is large, it may cause a considerable position error of the connecting point between the ballistic and pendulum trajectories. In this case, the directions of both the wire and the velocity of the ball at the connecting point are no longer perpendicular to each other. Hence an impact may be applied to the ball because its motion is restricted by the wire. As a solution for this problem, we expect that the SSB system can reduce the effect of this impact. We will address this matter in the future.

VI. CONCLUSION

In this paper, we first discussed how to apply force to an object to generate its initial high speed instantaneously. We then proposed a method of moving the object in the air by coordinated motion of swing of the arm and wind of the wire. Focusing on the merits and drawbacks of the spring, we developed the mechanical device that changes the apparent elasticity of the wire. We also developed a motion generator that provides an optimal collection motion. In simulation, we verified that the ballistic motion of the object was transformed into a dynamic stable state. Finally, we conducted experiments with the hardware and realized the motion of collecting a ball within a short time.

Future Works include development of high-speed vision system to detect the object's position, and the visual feedback control to reduce its position error at the end of each swing of the arm with modifying its trajectory.

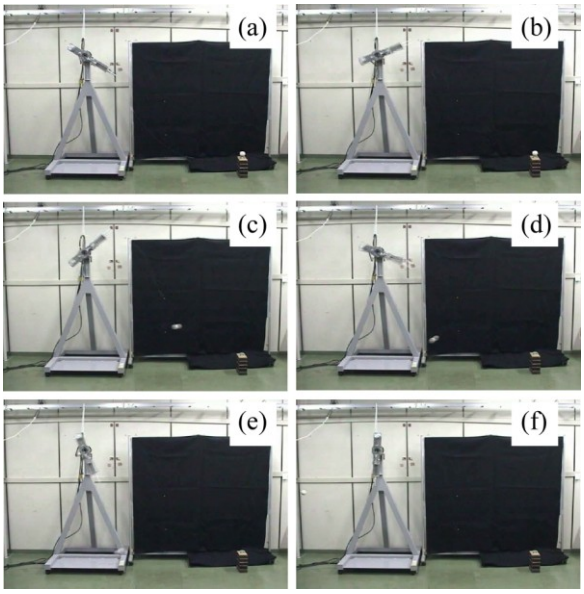

Fig. 17. Photo-sequence of the experiment.

REFERENCES

[1] Arisumi, H., Kotoku, T., Komoriya, K., "Swing Motion Control of Casting Manipulation," IEEE Control Systems, vol.19-4, pp.56-64, August 1999.

[2] Arisumi, H., Kotoku, T., Komoriya, K., "Study on Casting Manipulation (Experiment of Swing Control and Throwing)," Proc. of the IEEE/RSJ International Conference on Intelligent Robots and Systems (IROS'98), pp.494-501, 1998.

[3] Arisumi, H. and Komoriya, K., "Casting Manipulation (Midair control of gripper by impulsive force)," Proc. of the IEEE/RSJ International Conference on Intelligent Robots and Systems (IROS'99), vol.1, pp.291-298, 1999.

[4] Fagiolini, A., Arisumi, H., and Bicchi, A., "Visual-based feedback control of Casting Manipulation," Proc. of the IEEE International Conference on Robotics and Automation (ICRA'05), pp. 2203-2208, 2005.

[5] Arisumi, H. and Komoriya, K., "Catching Motion of Casting Manipulation," Proc. of the IEEE International Conference on Robotics and Automation (IROS'00), vol.3, pp.2351-2357, 2000.

[6] R. Souissi and A.J. Koivo: "Modeling and Control of Two Co-Operating Planer Crane," Proc. of the IEEE Int. Conf. on Robotics and Automation, pp.957–962, 1993.

[7] S. Kawamura, W. Choe, S. Tanaka and S. R.Pandian: "Development of an Ultrahigh Speed Robot FALCON using Wire Drive System," IEEE Int. Conf. on Robotics and Automation, pp.215-220, 1995

[8] Wen-Teng Cheng, "Synthesis of Universal Motion Curves in Generalized Model," Journal of Mechanical Design, Volume 124, Issue 2, pp. 284-293, 2002

[9] H. Makino, "Unsymmetrical Cam Curves for Two-Dwell Motion," Reports of the Faculty of Engineering, Yamanashi Univ., No. 20, pp41-50, 1969. (in Japanese)

[10] Shmuel S. Oren, and David G. Luenberger, "Self-Scaling Variable Metric (SSVM) Algorithms Part I: Criteria and Sufficient Conditions for Scaling a Class of Algorithms," MANAGEMENT SCIENCE, Vol. 20, No. 5, 1974.